Report Title:
Staged, High-Pressure Oxy-Combustion Technology:
Development and Scale-Up

Type of Report: Topical Report

Reporting Period Start Date: 10/01/2013

Reporting Period End Date: 09/30/2014

Principal Author(s)
Richard Axelbaum (PI)
Fei Xia
Akshay Gopan
Benjamin Kumfer

Report Issued: 12/31/2014

DOE Award Number: DE-FE0009702

Submitting Organization:
Washington University in St. Louis
One Brookings Dr.
Saint Louis, MO 63130

ABSTRACT

Washington University in St. Louis and its project partners are developing a unique pressurized oxy-combustion process that aims to improve efficiency and costs by reducing the recycling of flue gas to near zero. Normally, in the absence of recycled flue gas or another inert gas, combustion of fuel and oxygen results in a dramatic increase in temperature of the combustion products and radiant energy, as compared to combustion in air. High heat flux to the boiler tubes may result in a tube surface temperatures that exceed safe operating limits. In the Staged Pressurized Oxy-Combustion (SPOC) process, this problem is addressed by staging the delivery of fuel and by novel combustion design that allows control of heat flux. In addition, the main mode of heat transfer to the steam cycle is by radiation, as opposed to convection. Therefore, the requirement for recycling large amounts of flue gas, for temperature control or to improve convective heat transfer, is eliminated, resulting in a reduction in auxiliary loads.

The following report contains a detailed summary of scientific findings and accomplishments for the period of Oct. 1, 2013 to Sept 30, 2014. Results of ASPEN process and CFD modelling activities aimed at improving the SPOC process and boiler design are presented. The effects of combustion pressure and fuel moisture on the plant efficiency are discussed. Combustor pressure is found to have only a minor impact beyond 16 bar. For fuels with moisture content greater than approx 30%, e.g. coal/water slurries, the amount of latent heat of condensation exceeds that which can be utilized in the steam cycle and plant efficiency is reduced significantly.

An improved boiler design is presented that achieves a more uniform heat flux profile. In addition, a fundamental study of radiation in high-temperature, high-pressure, particle-laden flows is summarized which provides a more complete understanding of heat transfer in these unusual conditions and to allow for optimization. The results reveal that for the SPOC design, absorption and emission due to particles is the dominant factor for determining the wall heat flux. The mechanism of “radiative trapping” of energy within the high-temperature flame region and the approach to utilizing this mechanism to control wall heat flux are described. This control arises, by design, from the highly non-uniform (non-premixed) combustion characteristics within the SPOC boiler, and the resulting gradients in temperature and particle concentration. Finally, a simple method for estimating the wall heat flux in pressurized combustion systems is presented.

TABLE OF CONTENTS

EXECUTIVE SUMMARY

The requirement of high pressure CO_2 for sequestration or enhanced oil recovery (EOR) enables *pressurized combustion* as a tool to increase efficiency and reduce costs associated with carbon capture. In brief, the primary benefits of pressurized oxy-combustion include: 1) the moisture in the flue gas condenses at higher temperature, and thus the latent heat of condensation can be utilized to improve the overall cycle efficiency, 2) the gas volume is greatly reduced; therefore, the size and cost of equipment can be reduced, 3) at higher pressure, the convective heat transfer to boiler tubes is increased, for a given mean velocity, and 4) air ingress, which normally occurs in induced-draft systems, is avoided, thereby increasing the CO_2 concentration of the combustion products and reducing purification costs.

Washington University in St. Louis and its project partners are developing a unique pressurized oxy-combustion process that aims to further improve the efficiency and costs by reducing the recycling of flue gas to near zero. Normally, in the absence of recycled flue gas or another inert gas, combustion of fuel and oxygen results in a dramatic increase in temperature of the combustion products and the radiant energy, as compared to combustion in air. High heat flux to the boiler tubes may result in a tube surface temperature that exceeds safe operating limits. In the Staged Pressurized Oxy-Combustion (SPOC) process, this problem is addressed by staging the delivery of fuel and by novel combustion design that allows control of heat flux. In addition, the main mode of heat transfer to the steam cycle is by radiation, as opposed to convection. Therefore, the requirement for the recycling of large amounts of flue gas, for temperature control or convective heat transfer, is eliminated, resulting in a reduction in auxiliary loads.

During Phase I (FY13) of this project (DE-FE0009702), a system performance and techno-economic analysis of the SPOC process was conducted. Previous studies conducted by NETL have indicated that the penalty in plant efficiency due to implementation of first-generation (atmospheric pressure) oxy-combustion technology is approx. 10 percentage points. For the SPOC process, the resulting penalty is substantially reduced to approx. 3 percentage points, leading to a sizeable reduction in cost of electricity.

The following report contains a detailed summary of scientific findings and accomplishments resulting from this award during the period of Oct. 1, 2013 – Sept 30, 2014. This period represents the first year of Phase II activities, which will continue until Sept. 2016. The main objectives of Phase II are to conduct key experiments to develop, test and demonstrate the SPOC process and mitigate the risks and uncertainties identified during Phase I. A collateral objective is to validate that staged oxy-combustion holds promise over alternative approaches, such as flue gas recycle or coal-water slurry combustion, to control the heat flux associated with oxy-combustion while improving plant efficiency and minimizing equipment, operational and maintenance costs. Specifically, the focused R&D effort is to design and build a laboratory-scale facility and conduct laboratory-scale experiments and complimentary modeling that enable the SPOC technology for next-phase pilot scale testing.

During the reporting period, efforts were focused on the development of a 100 kWth test facility that is suitable for the study of pulverized coal combustion at elevated pressure (e.g. 15 bar) and in atmospheres with very high oxygen concentration. This facility has a flexible design to experimentally simulate the conditions in each stage of the SPOC process. Since construction of this facility is still ongoing, experimental results are not reported herein. The focus of this report is instead on the results from parallel modelling activities aimed at improving the SPOC process and boiler design.

Using the ASPEN Plus model, a parametric study was conducted to determine the effects of pressure and fuel moisture on the SPOC system performance. It is concluded that combustor pressure has only a minor impact beyond 16 bar. Increasing the combustor pressure leads to a negligible increase on the amount of flue gas moisture condensation and only a small increase of the heat available for integration with the Rankine cycle. In the range of pressures considered (16-36 bar), the increase in plant efficiency is quite modest (~ 0.14 percentage points). This increase is due to the shift of the location of the heat integration from the low-pressure region to the high-pressure region of the Rankine cycle, along with an increase in the heat available from the compression of oxygen.

Fuels with moisture contents ranging from 10 – 45% were considered. The results show that increasing moisture in the fuel reduces the net plant efficiency. When the moisture content is approx. 30%, the amount of latent heat of condensation exceeds that which can be utilized in the steam cycle for low-temperature heating of boiler feedwater, and plant efficiency falls rapidly with further increases in fuel moisture. Therefore, slurry feeding of fuel is not recommended.

Improvements to the conceptual full-scale boiler design are outlined and the distributions of temperature and wall heat flux, as predicted by CFD modelling, are presented. Design changes were implemented to achieve a more desirable flame shape, resulting in a uniform and controlled wall heat flux.

A fundamental study of radiation in high-temperature, high-pressure, particle-laden flows was conducted to provide a more complete understanding of heat transfer in these unusual conditions and to allow for optimization. At pressures relevant to SPOC, the combustion flue gas becomes very optically thick, due to the increase in char and ash particle volume fraction. Under these unique conditions, absorption and emission due to particles is a dominant factor for determining wall heat flux. A mechanism is found to exist for “trapping” radiant energy within the high-temperature flame region, and controlling wall heat flux. This control arises, by design, from the highly non-uniform (non-premixed) combustion characteristics within the boiler, and the resulting gradients in temperature and particle concentration. To illustrate this phenomenon, a 1-D analytical model was developed and results for wall heat flux are presented as a function of combustion pressure. Finally, a simple method for estimating the wall heat flux in pressurized combustion systems is presented.

METHODS

Process Modeling

A process model was developed using the ASPEN Plus (v8.0) platform. This work follows the National Energy Technology Laboratory (NETL) Quality Guidelines for Energy Systems Studies [1-4]. For all cases, the plant is assumed to be 550 MW_e with a supercritical Rankine cycle – 241bar/593°C/593°C (3500psig/1100°F/1100°F). Previously, results for PRB coal with supercritical and advanced ultra-supercritical steam conditions, as well as Illinois bituminous coal were reported. More recently, the effects of pressure and fuel moisture on plant efficiency were investigated in more detail. Only sub-bituminous Powder River Basin coal was considered (proximate and ultimate analysis given in Appendix). The modeled process achieves 90% capture of carbon dioxide produced by coal combustion, and the final CO_2 purity meets the required specifications for enhanced oil recovery. Details regarding the site conditions and final CO_2 purity are given in the Appendix. The condenser pressure was set as 0.48 bar. Gas and steam process flow diagrams are shown in Figures 1 and 2, respectively. A detailed description of the Staged, Pressurized Oxy-Combustion (SPOC) process is provided in ref [5].

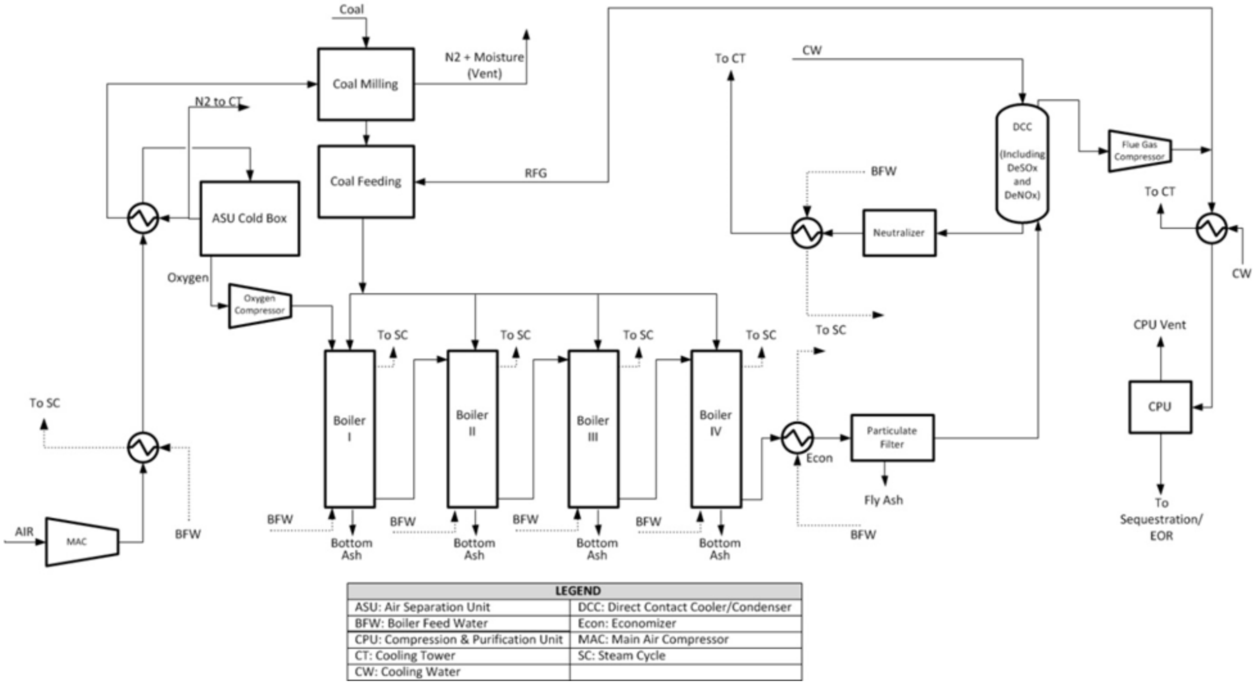

Figure 1: SPOC Process Flow Diagram: Gas Side

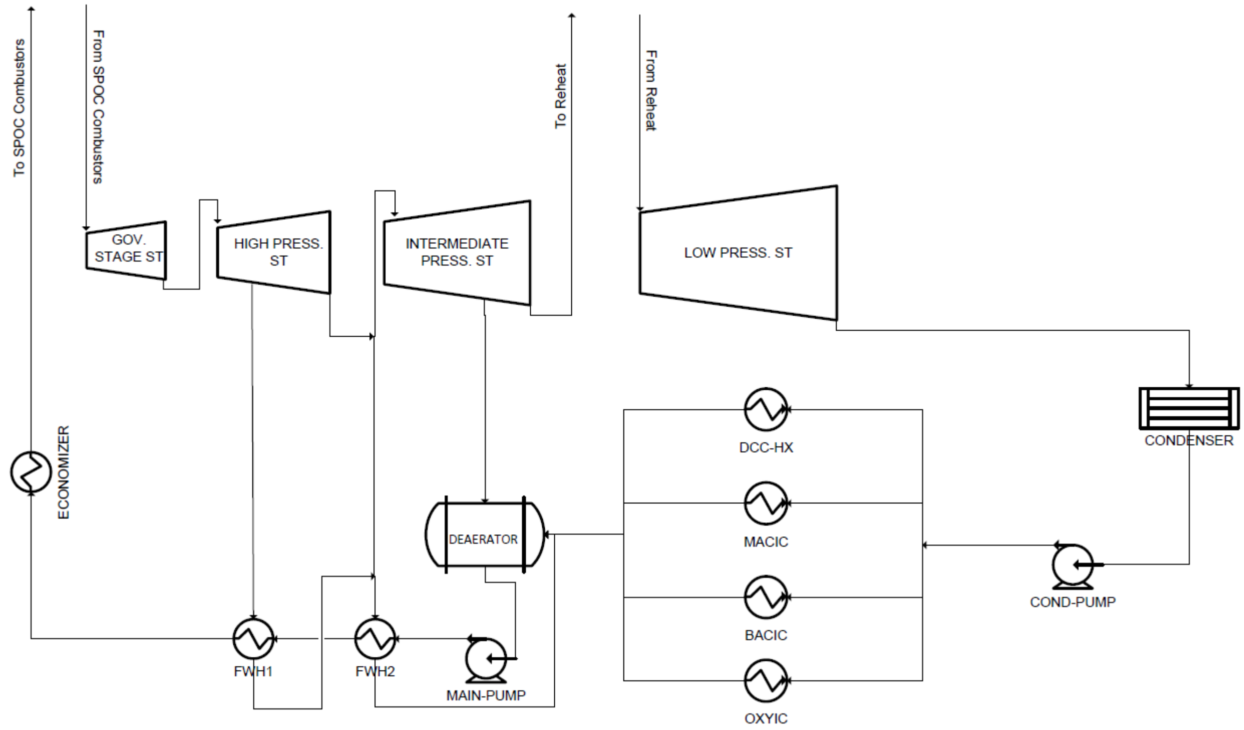

Figure 2: SPOC Process Flow Diagram: Steam Side. (DCC-HX: heat exchanger recovering heat from the Direct Contact Column; MACIC: ASU Main Air Compressor Intercooler; BACIC: ASU Booster Air Compressor Intercooler; OXYIC: ASU Oxygen Compressor Intercooler

For the gas side modeling, the Peng-Robinson equation of state was used. For SO_x and NO_x removal, the ENRTL-RK method (ENRTL activity coefficient method with RK equation of state) was used so as to model the stream of dilute acid formed in the direct contact cooler (DCC). For the steam side (Rankine cycle), STEAM-TA (steam tables) was used.

Computational Fluid Dynamics Modeling

ANSYS FLUENT version 13.0 was used for this study. The flow field was modeled applying the Reynolds Averaged Navier Stokes (RANS) equations with the Semi-Implicit Method for Pressure Linked Equations (SIMPLE) algorithm to address pressure-velocity coupling. RANS has been used extensively to study the flame behaviors of pulverized fuel [6-8]. The sub-models for solid fuels combustion have been extensively validated for scales from laboratory to industrial [9-15]. It has been shown that RANS is able to provide reasonable agreement between experiments and CFD simulations.

Turbulence and turbulent interaction models

In turbulent combustion simulations, modeling the turbulence is one of the most significant considerations. Serious limitations have been observed for the $k-\varepsilon$ model in the near-wall region. This model over predicts the turbulence scale for flows with adverse pressure gradients, which leads to higher heat transfer rates and wall shear stress [16]. It is a great advantage to use the $\omega-$equation in the near wall region. However, the solution of the standard $k-\omega$ model is strongly sensitive to the free stream values of ω outside the boundary layer [17]. To address the problems associated with standard $k-\varepsilon$ and standard $k-\omega$ models, the shear stress transport (SST) $k-\omega$ model has been developed to combine the best of the two eddy-viscosity models [18]. The SST $k-\omega$ model is used in this simulation.

The turbulence-chemistry interactions are another significant consideration in turbulent combustion modeling. The Eddy Dissipation Model (EDM) [19, 20] was utilized in this simulation, as it has been successfully used in oxy-coal combustion modeling [21]. In the EDM, the chemical reaction rate is determined by the large-eddy mixing time scale (k/ε). The reaction rate in the EDM is limited by the mixing rate of reactants and the heating rate of reactants via the mixing with the products.

Coal combustion models

The trajectories of particles was computed in a Lagrangian frame and coupled to the gas phase in the Eulerian frame. With this approach, mass, momentum, and energy are exchanged between the two phases. All discrete particles that were injected into the system were assumed to be spherical. The pulverized coal particle size was assumed to follow the Rosin-Rammler distribution, with an average diameter of 65 μm.

The Chemical Percolation Devolatilization (CPD) model [22] was used to calculate the thermal decomposition rate of the coal particles. NMR chemical structure parameters were calculated according to the correlations in [23]. Ultimate and proximate analyses were applied to determine the chemical properties of volatile matter. The oxidization of volatile gases was modeled using a two-step reaction mechanism with wet combustion [24]. The kinetic/diffusion-limited rate model was applied for char surface reactions. This model assumes that the surface reaction rate is limited by the kinetic rate and diffusion rate. FLUENT applies the models from [25, 26].

Radiation model

Radiation is the dominant heat transfer mode in the combustion environment at such high temperatures with hot solid particles participating in the radiation heat transfer. Since particle radiation from coal, char, and ash can contribute significantly to radiation heat transfer, its contribution was also considered by including the particle absorption and scattering effects in the radiative transfer equation (RTE) [27]. The Discrete Ordinates (DO) [28, 29] radiation model was used in this simulation to solve the RTE, with each octant being discretized into 4x4 solid angles. Gaseous absorption was considered by a domain-based Weighted Sum of Gray Gases model (WSGGM).

Discrete phase model

In FLUENT, the discrete phase model (DPM) was applied to compute the particle trajectories and to determine the mass and energy transfer to and from the particles, with two-way coupling between the discrete phase and the continuous phase. The effect of turbulence on the particle trajectories was accounted for with the Discrete Random Walk (DRW) model. The particle thermophoretic velocity for SPOC was calculated to be on the magnitude of 10^{-5} m/s based on the expression in [30]. Therefore the thermophoretic force was ignored in the CFD simulation.

RESULTS AND DISCUSSIONS

Process Modeling: Effects of Pressure and Fuel Moisture

Operating Pressure

Based on equilibrium flash calculations, the amount of moisture condensation increases by less than 1% upon increasing the pressure from 10 bar to 35 bar, for flue gas temperature less than 50°C. At any given exit temperature, the effect of pressure on moisture condensation is of diminishing returns with increasing pressure.

Since the analysis of the DCC indicates that 15 bar is sufficient to capture the large majority of the latent heat, the minimum operating pressure of the radiant boilers considered in this study is 16 bar, to allow for pressure losses between the boilers and the DCC. Furthermore, the integrated SO_x and NO_x removal processes have been indicated to work best at pressures 15 bar and higher [31]. This consideration allows for avoiding any moving parts (compressors) between the radiant boilers and the DCC.

Three pressure cases in the 16 bar to 36 bar range were considered. An increase in combustion pressure above 16 bar increases the net plant efficiency only slightly, and with diminishing returns, as can be seen in Figure 3. The difference in net plant efficiency between 16 bar and 36 bar cases is less than 0.14 percentage points. The different contributors to this trend are discussed below.

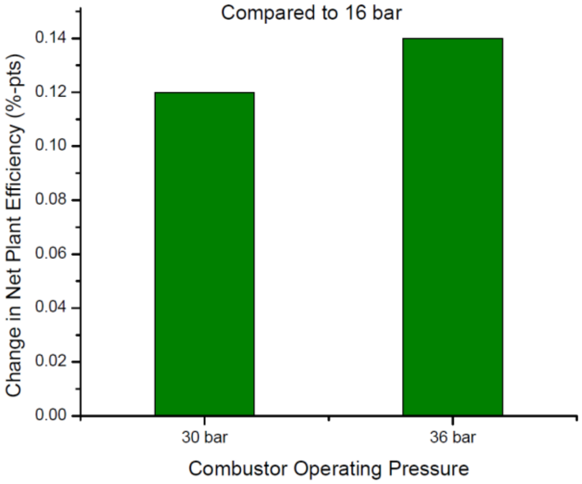

Figure 3: Increase in net plant efficiency (HHV) with combustion pressure, as compared to 16 bar.

The power requirement for oxygen production increases with the combustion pressure. Since this increase in power demand is only for increased compression, and since the final flue gas is required to be compressed up to 153 bar, the CPU power load is reduced. The sum of ASU and CPU power demand, on the other hand, remains relatively constant, between 142 – 145 MWe (≈ 0.09MWe/MWt fuel input), for all three pressures cases. In SPOC, heat from either flue gas moisture condensation or "waste heat" from auxiliary systems can be integrated into the steam cycle, thereby reducing the steam extraction requirement for regeneration of boiler feed water (BFW). Even though, in a Rankine cycle, reduction in steam extraction for feedwater heating (regeneration) results in a lower cycle efficiency, the extra heat addition to the cycle from the DCC and the auxiliary systems increases the overall (net) plant efficiency. With increasing pressure, the temperature of the DCC bottoms product (hot water with small quantity of acids) increases. DCC heat was partially integrated into the higher pressure BFW regenerators, as the DCC bottoms temperature increased from 170°C to 193°C and 200°C, with increasing combustor (and DCC) pressure from 16 bar to 30 and 36 bar. This partial shift in integration of DCC heat allows for the extra heat available from oxygen compression, at higher pressures, to be integrated into the low pressure BFW regenerators. Increasing pressure, not only increases the range in which heat is available from the DCC, but also the amount of water required in the DCC. This reduces the heat rejected after heat transfer to the BFW.

With increasing pressure, more heat is available from the ASU. The partial shift of DCC heat into the HP region allows the increased heat transfer from the ASU into the steam cycle, thus increasing the net plant efficiency (Figure 3). Still, since the temperature at which heat available from oxygen compression is restricted, the benefit from increasing pressure is of diminishing returns.

Fuel Moisture

In order to feed the coal into the boilers at elevated pressure, a high pressure, dense-phase feeding system (pneumatic dry feeding) has been considered in the process analysis. This process requires that the surface moisture of the pulverized coal be removed for optimal feeding. Further drying to remove some inherent moisture may also be considered. An alternative method to feeding the coal is to produce coal water slurry, which can be readily pumped to deliver the coal at elevated pressure.

A systematic study on the effect of as-fired moisture on net plant efficiency was performed by studying 6 different cases. The as-received coal moisture is 27.42%. In 3 cases, drying to 9.7%, 17% and 24% moisture are considered. The other three cases represent moisture addition to the as-received fuel (30%, 35%, 45%). Other parameters of the process were kept constant. The drying of coal was modeled as being performed by dry nitrogen gas from the ASU. The heat for coal drying was partly derived from ASU, and partly from previously unutilized low temperature heat from CPU boost compressors (for drying beyond 17% fuel moisture).

As can be seen from Figure 4, the net plant efficiency monotonically decreases with increasing moisture content, but the slope of the curve changes drastically between the low moisture and high moisture cases. In the low moisture cases, low pressure BFW is heated with a combination of auxiliary heat and steam extraction. With increasing amounts of moisture in the fuel, the heat available from the radiant boilers and the economizer is reduced, whereas the amount of heat available from the DCC increases. Overall, this shift of heat from the high grade to the low grade reduces the amount of steam extraction for BFW regeneration in the low pressure regenerators. The sum of the heat available from the boilers and the DCC is almost constant at low moistures, and so is the heat available from other auxiliary systems like ASU and CPU for a given fuel input. Since the net heat supplied to the steam cycle is constant, but the steam extraction is reduced, the cycle efficiency reduces, and so also the plant efficiency. The reduction in plant efficiency is only slight. As the fuel moisture increases further, more heat is available from the DCC for integration and the steam extraction from the LP steam turbine is eliminated. This is considered the point of “heat saturation” of the LP BFW. Increasing fuel moisture further leads to no additional heat integration into the Rankine cycle from the DCC. This “heat saturation” point is around 29% as-fired moisture for the system modeled here. Beyond the point of “heat saturation”, increasing fuel moisture does not reduce the cycle efficiency significantly, but the net plant efficiency reduces. This is because the heat from the boilers is significantly reduced with increasing moisture, and the equivalent heat is not even available as low grade heat from the DCC. This reduces the net heat supplied to the steam cycle, and with a lower efficiency cycle (no steam extraction for BFW regeneration), the net plant efficiency reduces drastically. The excess heat from the DCC condensate, which cannot be integrated into the steam cycle due to “heat saturation” needs to be cooled using cooling water and discarded.

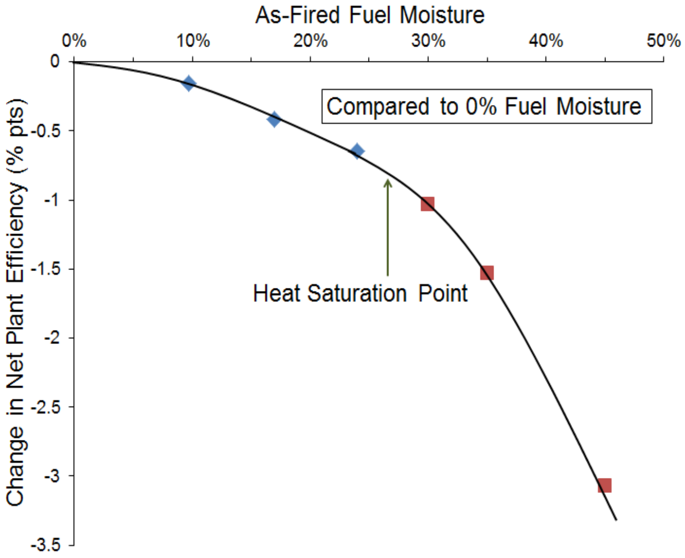

Figure 4: Effect of as-fired fuel moisture on net plant efficiency

In most conceptual pressurized systems modeled, coal water slurry feeding is considered as the standard approach for fuel feeding due to the available experience and expertise in such feeding for other purposes, such as coal gasifiers. These pressurized systems are considered to be more beneficial for low rank coals as the hitherto unrecovered heat of moisture condensation may potentially make them less inefficient. In the above paragraphs, it has been shown that increasing the moisture content beyond what would lead to LP BFW “heat saturation” is detrimental to the plant efficiency. Previous work by the same group [23] highlights the starkness of the problem if low rank coal-water slurry feeding is considered as the means for coal delivery. In order to pump slurry, the maximum apparent viscosity accepted in the industry is about 1000 mPa-s at 100s-1 [24, 25]. The viscosity of the CWS increases with the hydrophilicity of the coal. Therefore, a hydrophobic coal can more easily form low viscosity slurry at high solids loadings. Normally, high-rank coals are hydrophobic, while low-rank coals are hydrophilic [26]. For high pressure operations, like coal gasification, coal water slurry feeding technique works well for bituminous coals but not for lower grade coals [27]. Delivering coal water slurry using PRB coal requires water content as high as 65 wt% in order to make it pumpable [23].

The results of this work show that increasing moisture in the fuel reduces the net plant efficiency. This is more apparent in fuels with inherently high moisture content. The inability to integrate the latent heat of condensation of fuel moisture for such cases would significantly reduce the plant efficiency (compared to surface-dry feeding). Thus, slurry feeding of fuel even in high pressure combustion processes is not recommended. On the other hand, drying the fuel (beyond the minimum requirement for dry feeding) does not increase the efficiency significantly either.

CFD-Aided Design and Analysis of Pressurized Radiant Boilers

During Phase I (FY13) of this project, a preliminary design of the radiant boiler for a conceptual 550 MWe SPOC plant was proposed and analyzed. In this period, this design was further improved using CFD modelling to result in a more uniform heat flux profile. In the CFD results described below, the combustion pressure was set to 15 bar. Detailed boiler operating conditions, such as the inlet flows and gas composition, can be found in the Appendix and ref [32].

As shown in Fig. 5, a tapered geometry has been incorporated in the combustion zone, in contrast to previous designs which featured a constant inner diameter. The tapered geometry was implemented to improve flame shape and maintain optimal heat flux in the near-burner zone. Note that while the boilers are to be down-fired and oriented vertically in practice, they are shown horizontally in Fig. 5. The direction of the gravity force is noted in Fig 5. Shown are the temperature distributions for all four SPOC stages. The temperature contours are typical of long jet flames. This flame shape is desirable as the heat release from combustion is distributed along the length of the boiler, and combustion is made to occur near the center of the boiler and away from the boiler tube walls. This flame shape provides manageable levels of radiant heat transfer to the wall, as demonstrated in Fig. 6. Note that in this simulation, the wall emissivity was set equal to one, therefore, the heat flux levels in Fig. 6 are conservatively high. The heat flux in the combustion zone is highest in Stage 1, in which coal (fed using CO_2) is burned in an atmosphere of nearly pure oxygen at a stoichiometric ratio of four. Locations with very high local temperature (>2500 K) are also found in Stage 1. Despite the high temperature, the resulting heat flux to the wall is maintained to within limits of advanced boiler tube materials (< 650 kW/m2). This result is largely due to the presence of excess oxygen, which acts as a diluent and helps to control flame shape, and the effects of elevated pressure on the radiative properties of the particle-laden gases, which is discussed in detail in the following sections.

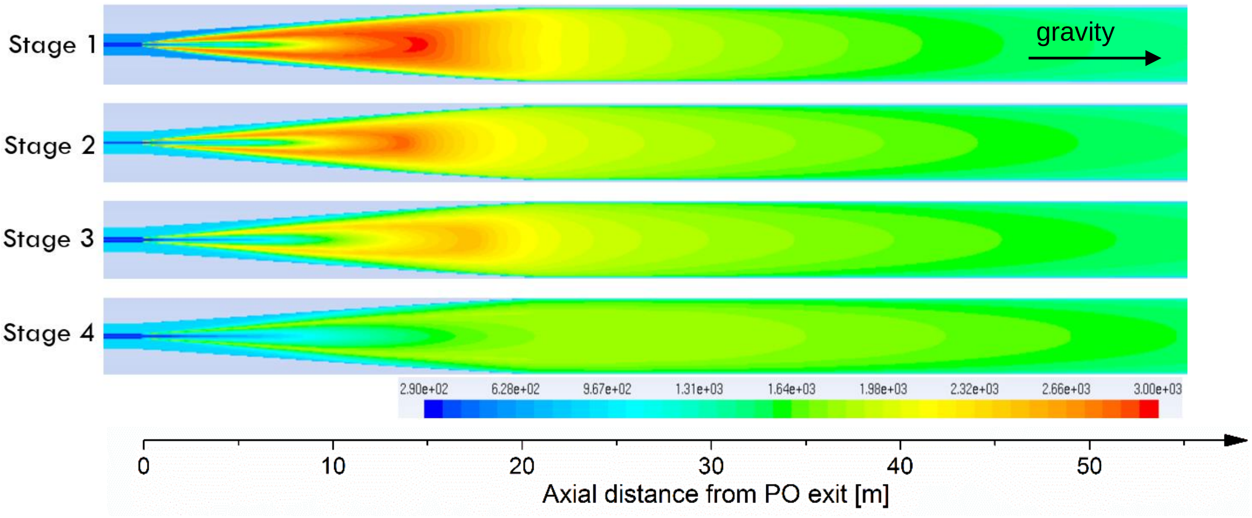

Figure 5: Temperature (K) distributions of improved SPOC design for stages 1-4.

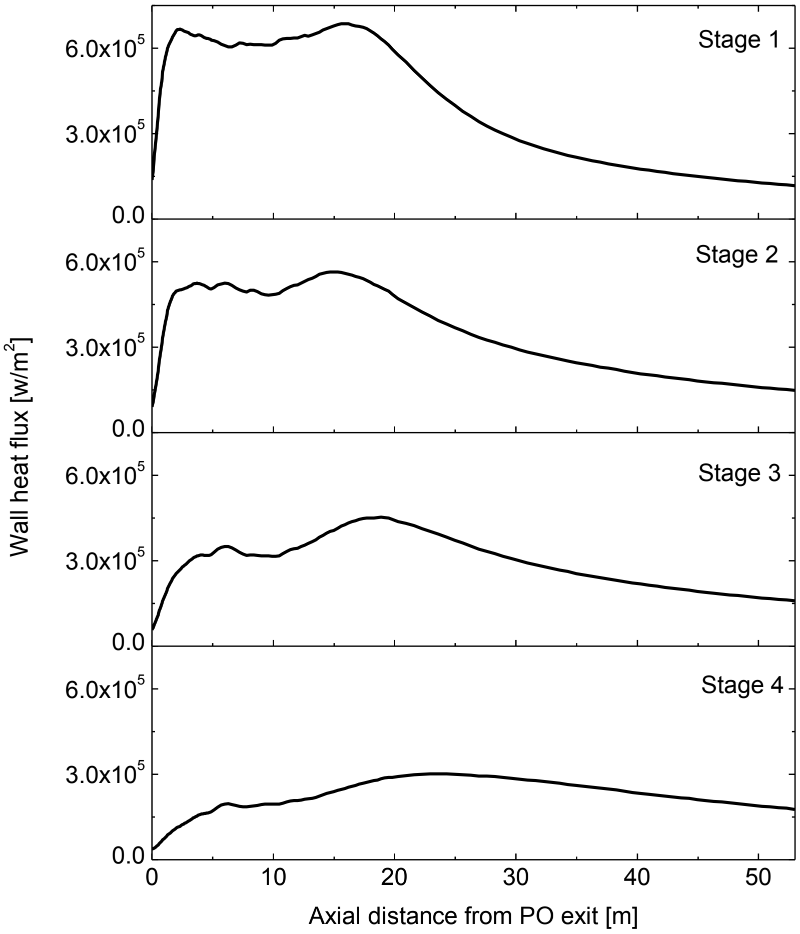

Figure 6: Wall heat flux (W/m2) for Stages 1-4

Radiative trapping effects in SPOC system

The fact that relatively manageable wall heat flux was obtained under flame temperature as high as around 3000 K can be explained by absorption due to ash particles outside the flame. For a cloud of particles, the absorption coefficient k_a is given by

$$k_a = \sum_{i=1}^{n} N_i Q_a \pi \frac{D_i^2}{4} = \frac{3}{2}\sum_{i=1}^{n} Q_a \frac{f_{v,i}}{D_i} \ , \qquad (1)$$

where N_i, D_i , and $f_{v,i}$ are the number of particles per unit area, the diameter, and the volume fraction of the *i*th particle, respectively. Q_a is the absorption efficiency factor [33]. This parameter also refers to the equivalent absorption coefficient due to particles in the Discrete Phase Model (DPM) used in FLUENT [27].

A numerical test was conducted to show the effects of particle absorption in the first stage of the SPOC system. In this case, the optical properties of particles in the hot flame zone (defined as the area where temperature is greater than 2500K) remained the same as in previous cases, but particles outside the flame zone were assumed to be transparent with no emission, absorption and scattering ability. Fig. 7 shows the equivalent particle absorption coefficient contour for this case as compared to the previous case with realistic optical properties for particles. As shown, the average absorption coefficient of the particle cloud outside the flame in the realistic case is around 7.5 1/m, which is about 15 times of the average particle cloud absorption coefficient in a typical atmospheric air-fired coal combustion boiler. This is because the elevated pressure in SPOC increases the particle number concentration in the system. On the contrary, the absorption coefficient of the medium outside the flame zone for case (a) in Fig. 7 is near zero.

Simulation results show that the two cases have similar flame shape and temperature distribution, but the wall heat fluxes in the two cases differ substantially, as shown in Fig. 8. It is normally expected that wall heat flux will increase due to the presence of solid particles, since they are typically strong emitters, which is true for case (a). Without high number concentration of ash particles between the flame hot zone and the wall to act as radiative trapping medium in case (a), the very high emissive power from the hot flame can easily reach the wall, leading to wall heat flux as high as 1100 kW/m^2. However, when both the optical behavior of ash particles and particle radiation interactions are considered in the model, the maximum wall heat flux of cases (b) decreases to a manageable level of about 600-650 kW/m^2. Clearly, due to their absorption effects, particles are responsible for the lower peak wall heat flux for the case (b). Another point to notice is that wall heat flux of case (b) is distributed in a more uniform way due to radiative trapping, which makes the downstream mean temperature higher, and in turn contributes more to the wall heat flux.

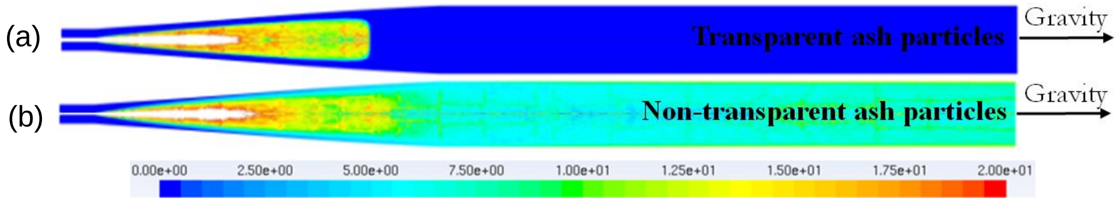

Figure 7: DPM absorption coefficient for cases (a) with transparent particles, and (b) non-transparent particles outside flame zone.

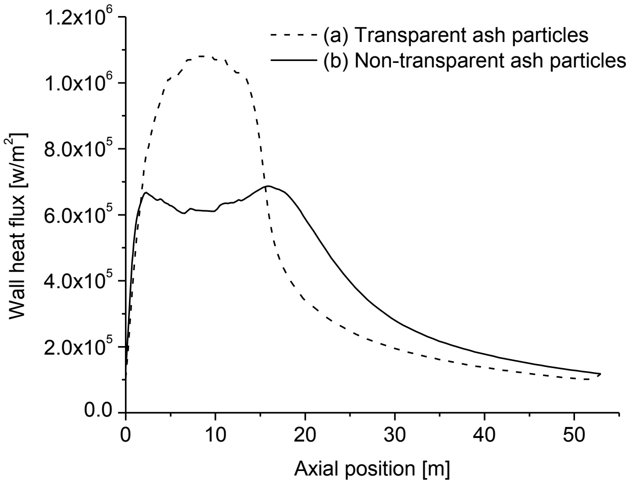

Figure 8:Wall heat flux comparison cases with (a) with transparent particles, and (b) non-transparent particles outside flame zone.

Fundamental Study of Radiation Heat Transfer during Pressurized Combustion

Effect of absorption coefficient on radiative trapping

A fundamental study was conducted to understand how pressure and gradients in temperature and particle concentration can influence the radiation behavior of a medium. For a system with emission, absorption, and scattering, the change in radiative intensity *I* along path *s* is given by

$$\frac{dI}{ds} = k_a I_b - k_a I - \sigma_s I + \frac{\sigma_s}{4\pi}\int_{4\pi} I(\hat{s}_i)\Phi(\hat{s}_i, \hat{s})\,d\Omega_i\,, \qquad (2)$$

where $I_b(T) = \sigma T^4 / \pi$, σ_s is the scattering coefficient, k_a is the total absorption coefficient, Φ is the scattering phase function, and Ω is the solid angle. The first and fourth terms on the right hand side of Eq. (2) are augmentation to the intensity due to local emission and scattering. The second and third terms correspond to the attenuation of radiation intensity due to absorption and scattering.

Because of the complex nature of radiative heat transfer processes, only a few very simple situations have exact analytical solutions. One of them is the case with known temperature and absorption coefficient profiles in a one-dimensional plane-parallel medium when scattering is ignored [34]. In the present study, a one-dimensional medium is used to study the effects of the absorption coefficient on radiative trapping phenomenon, and scattering is neglected to simplify the analysis.

The solution to Eq. (2) ignoring scattering is

$$I(\tau,\theta) = \frac{1}{\mu}\int_0^{\zeta} I_b(\zeta')e^{(\zeta'-\zeta)/\mu}d\zeta', \quad 0 < \mu < 1, \tag{3}$$

where $\mu = \cos\theta$, $\zeta = \int_s k_a ds$ is the optical thickness, and k_a is the absorption coefficient.

Eq. (3) shows that the local radiative intensity can be calculated if the temperature and the absorption coefficient profiles can be obtained. After integration over all angles, the heat flux at the location ζ in the direction towards the wall can be given as.

$$q^+(\zeta) = \int_0^{\tau} I_b(\zeta')E_2(\zeta-\zeta')d\zeta' , \tag{4}$$

where $E_n(x) = \int_1^{\infty} e^{-xt}\frac{dt}{t^n} = \int_0^1 \mu^{n-2}e^{-x/\mu}d\mu$.

Consider a layer of medium with 1 m thickness, which is a relevant length scale for large-scale boilers. As a first step uniform profiles for the absorption coefficient and temperature are used to simplify the problem. The temperature is 2000 K for all cases. Five values for the absorption coefficient are considered (0.5, 0.8, 2.5, 5 and 7.5 1/m), which correspond to the cases of air-fired combustion, typical oxy-combustion at atmospheric pressure, and oxy-combustion at pressures of 5, 10, and 15 bar, respectively. Results for the local heat flux in the *x* direction for the five cases are shown in Fig. 9. It can be seen that for cases with small absorption coefficients, the augmentation of medium emission is the dominant factor. The local heat flux continues to accumulate as *x* increases. Most of the radiation emitted from the left part of the medium can pass through the right part of the medium and reach the right boundary. For the cases with larger absorption coefficient, attenuation (i.e., absorption) by the medium becomes important. When the absorption coefficient is high enough, such as the case of oxy-combustion at 15 bar, the local heat flux quickly saturates to a value of σT^4, i.e., the medium behaves like a blackbody. At this condition of saturation, *transmission* of radiant energy becomes negligible, and the local radiant heat transfer at a given location is governed by the temperature at that location. It should be noted that, for the small absorption coefficient cases, as the medium thickness gets larger, the local heat flux also eventually reaches the same saturated value. In systems that have large absorption coefficients, the heat flux towards the wall increases much faster than for small absorption coefficients, and the maximum heat flux is reached in a shorter path length.

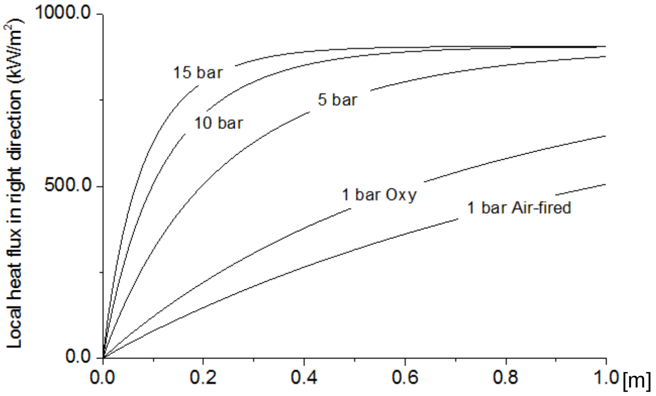

Figure 9: Local heat flux distributions towards the right boundary for a range of absorption coefficients, assuming uniform temperature distribution.

The above discussion suggests that when the optical thickness of the medium increases sufficiently to cause saturation, the local heat flux has reached a maximum value, and is only dependent upon the local conditions. For this case in which the temperature and absorption coefficient are uniform throughout the system, the heat flux to the right boundary is very high due to local high temperature.

Next conditions are considered that are more relevant to the SPOC boilers in which the temperature and absorption coefficient are not uniform. In order to observe the effects of variable absorption coefficient profiles, four profiles were defined, as shown in Figure 10. In each of the four cases, the same linear temperature distribution profile was assumed. For this example the temperature decreases linearly from 2600K at the left side to 700K at the right side. The left boundary represents the boundary of the high-temperature combustion zone, and the right boundary represents the boiler wall. By integrating the different absorption coefficient profiles along the medium thickness, the optical thickness profiles are obtained and plotted in Fig. 11, and the total optical thickness for these cases ranges from 0.2 to 6.4. For reference, when the optical thickness is equal to 2.3, the transmissivity is equal to 0.1 (i.e. $e^{-2.3} = 10\%$). This transmissivity value implies that 10% of the radiative energy arriving at this location is transmitted towards the wall.

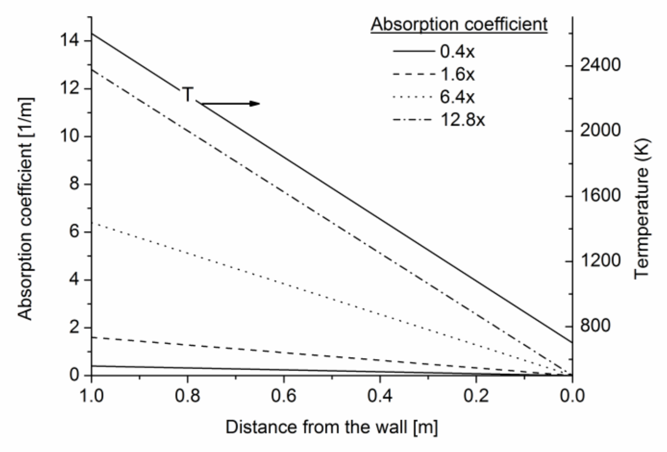

Figure 10. Absorption coefficient and temperature profiles assumed for the 1-D analysis.

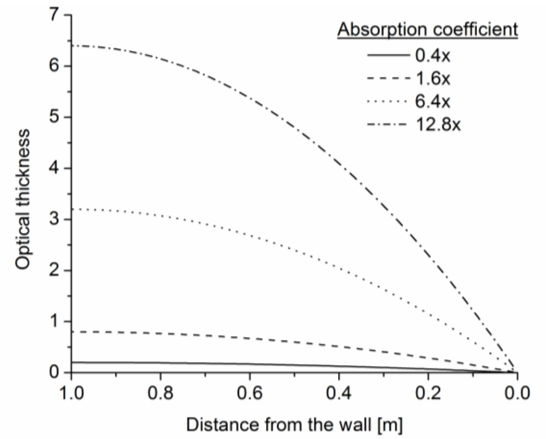

Figure 11: Optical thickness profiles

Figure 12 shows the distribution of the local heat flux in the *x* direction for the four cases. First, the case of low optical thickness is considered ($k_a(1) = 0.4$ in Figure 10). In this case the absorption by the medium is weak. As distance from the wall decreases from 1 (the high temperature boundary) to 0 (the low temperature boundary), the local heat flux gradually increases due to the augmentation of radiation emitted from high temperature zones. Still, the increase in the local heat flux is slow because the absorption coefficient is also small in this case. As distance from the wall is further decreased the heat flux profile becomes flat. At this condition, radiation originating from the higher temperature boundary is readily transmitted, and the local contribution to the emission is low due to lower temperature and emissivity.

When the absorption is increased ($k_a(1) = 1.6$), the emission and absorption by the medium both become stronger. In the high temperature zone, the local heat flux becomes much larger, but in the low temperature zone, the local heat flux begins to drop, because absorption starts to become significant. Note that in this case, the heat flux at the wall is approximately doubled as compared to the case of low absorption. When the optical thickness becomes even larger ($k_a(1) = 12.8$), the absorption effect in the low temperature zones becomes more intensive, and most of the radiation emitted from the high temperature zone is locally absorbed. This results in a drastically reduced heat flux at the wall. In this case of high absorptivity, the energy in the high temperature zone is effectively “trapped”, as only a fraction of this energy is transmitted to the wall. Hence, the term *radiative trapping* is used here to describe this phenomenon.

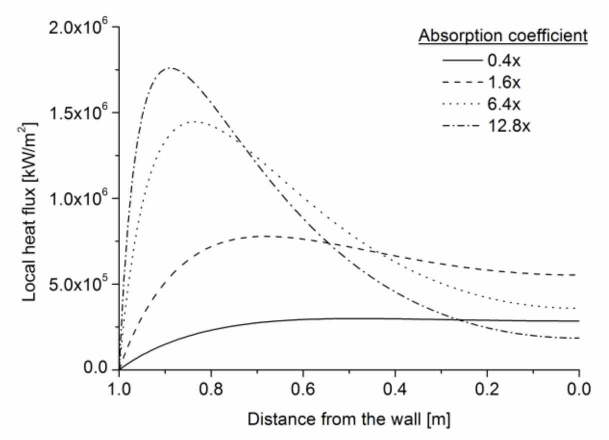

Figure 12: Local heat flux towards the right boundary (x=0) under the different absorption coefficient profiles

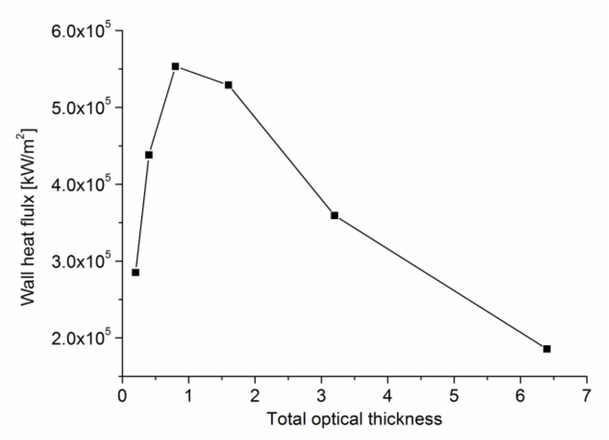

Figure 13: The surface incident radiation on the wall as total optical thickness varies

In Fig. 13, the surface incident radiation on the wall is plotted as a function of optical thickness. When the optical thickness is smaller than 1, the heat transfer process is controlled by the radiation augmentation in the high temperature zone, and thus the surface incident radiation at the cold side increases with optical thickness. When the optical thickness is larger than 1, absorption in the low temperature zone starts to control the process.

It is concluded from above discussion that the dynamic relationship between temperature and absorption coefficient throughout the domain determines the final wall heat flux at the wall. In other words, the temperature and absorption coefficient profiles will determine the relative amounts of local emission (augmentation) in the high temperature region, and local absorption (attenuation) in the low temperature region. By comparing Figs. 12 and 9, it is clear that the diffusive-convective type profiles of the temperature and absorption coefficient that allow for control of the wall heat flux in pressurized systems.

Average-temperature approximation method

It has been established that wall heat flux is dictated by the profiles of both the temperature and absorption coefficient. In this section, the dynamic relationship between temperature and the absorption coefficient on wall heat flux are studied for systems with an optical thickness larger than 2.3, and a new method, namely the average-temperature approximation (ATA) method, is developed to easily predict the radiation behavior of a diffusive-convective system.

Figure 14 shows simplified profiles of temperature and absorption coefficients where the flame is on the left and the wall is on the right. Two boundaries are identified by dashed lines. The boundary on the left corresponds to an optical thickness of 2.3, which means only 10% of the radiative energy arriving at this location is transmitted. In effect, radiative sources on the left of this boundary can be ignored in the calculation of wall heat flux. The boundary on the right corresponds to an optical thickness of 0.1, which means 90% of the radiative energy arriving at this location is transmitted. Basically this boundary indicates that absorption is negligible beyond this location, and almost all the radiative energy arriving at this point will be transmitted to the wall. Due to the characteristics of the diffusive-convective flow, the temperature near the right boundary is normally low, which makes the contribution of local emission in this zone negligible. Therefore, these two boundaries define an *effective* zone that determines the final value of the wall heat flux. The effective zone is shown in Figure 14 between the two boundaries marked with 10% and 90%. The average temperature in this zone is also indicated in Fig. 14.

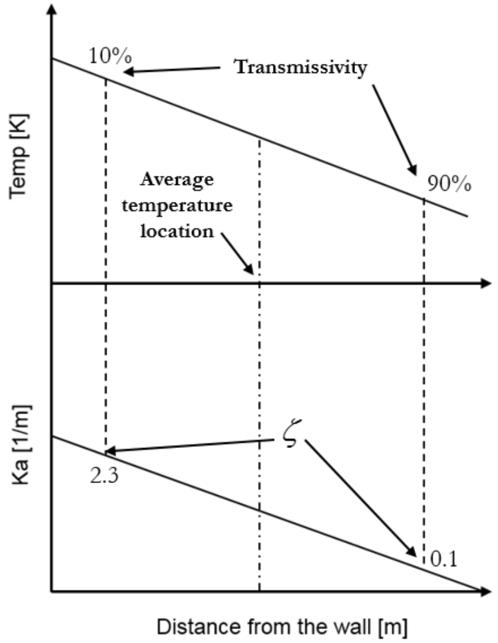

.

Figure 14: Temperature and absorption coefficient (ka) profiles showing boundaries for low and high transmission

According to Beer's law, the local effective wall heat flux ($q_{w,eff.}$) (w/m^2/m) can be expressed as

$$q_{w,eff.} = k_a * \sigma * T^4 * e^{-\zeta}, \quad (5)$$

where k_a is the absorption coefficient, σ is the Stefan-Boltzmann constant, T is the local temperature, and ζ is optical thickness of the path between the local position and the wall. In order to obtain an approximation of the wall heat flux, the average values for T and k_a are used in Eq. (5), as well as the length L_{eff} , which is defined as the distance between the two boundaries corresponding to 10% and 90% transmissivity. The wall heat flux then becomes

$$whf = \overline{k_a} * \sigma * \bar{T}^4 * L_{eff} * e^{-\zeta_{eff}}, \quad (6)$$

where $\overline{k_a}$ is average absorption coefficient, $\bar{T}$ is the average temperature, and ζ_{eff} is the effective optical thickness, which is a constant 1.1 (2.2/2) due to the two boundaries we defined. Since the multiplication of $\overline{k_a}$ and L_{eff} is simply 2 ζ_{eff} , the wall heat flux (*whf*) (w/m^2) equation now becomes

$$whf = 2 * \zeta_{eff} * \sigma * \bar{T}^4 * e^{-\zeta_{eff}} , \qquad (7)$$

Since both ζ_{eff} and σ are constant, the wall heat flux is determined only by $\bar{T}$.

$$whf = 4.152 * 10^{-8} * \bar{T}^4 . \qquad (8)$$

This approximation method is useful, because for any optically thick system, as long as the two boundaries can be identified, the average temperature in this zone can be used to approximate the wall heat flux. More importantly, the dynamic relation between the temperature and absorption coefficient can be described simply via the average temperature.

The application of the ATA method is illustrated in Fig. 15. Three different linear absorption coefficient profiles are plotted together with the same linear temperature profile. Dash lines correspond to the boundaries of 10% and 90% transmissivity, and dash-dot lines indicate the locations of average temperature. It is clearly shown that when absorption coefficient increases, the boundaries move to the right, which results in a decrease in average temperature. The wall heat flux decreases accordingly based on Eq. (8). A comparison between the exact solution and the ATA method for the three cases is shown in Table 1. The agreement is reasonable good for these three cases.

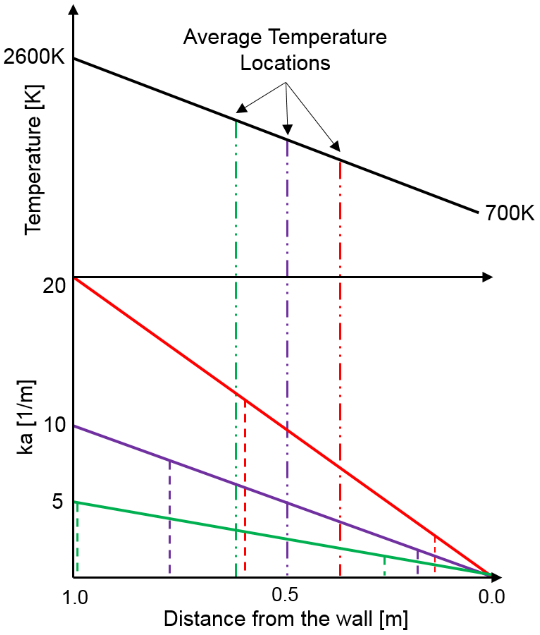

Figure 15: Illustration of the method of average-temperature approximation

Table 1. Comparisons between exact solution and average temperature approximation method

ka (1/m)	Wall heat flux (kW/m^2)	
	Exact solution	ATA method
Case 1: 5x	494	442
Case 2: 10x	219	200
Case 3: 20x	117	102

Application of the average temperature approximation (ATA) method

The ATA method is a useful design tool to estimate wall heat flux in optically dense diffusive-convective systems. This method was applied in the design of the SPOC boilers to estimate the wall heat flux and demonstrate its applicability in three dimensional problems.

Figures 16 and 17 show the temperature, equivalent particle absorption coefficient, and wall heat flux from the FLUENT simulation results. Five cross sections, distributed in the boiler, are represented in Fig. 16 by vertical black lines. Figure 18 shows the radial distributions of the temperature and equivalent particle absorption coefficient for these five sections. Because of the high particle number concentration near the centerline of the furnace, the equivalent particle absorption coefficient can be as high as 1000 1/m. Therefore, the profile of the equivalent particle absorption coefficient is truncated to show the region relevant to the wall heat flux. As expected, the gradients of the radial temperature and species concentration profiles gradually decrease with axial distance from the burner and finally reach a point of uniform distribution, as shown in Figure 18e. The maximum heat flux is observed in Fig. 17 at an axial position of around 16 m, where the flame diameter is largest. There is an additional peak in wall heat flux at an axial position of roughly 2 m due to the small path length to the wall with limited optical thickness to trap the heat.

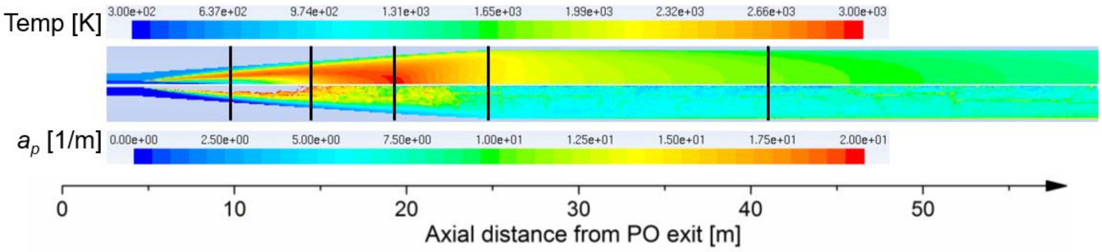

Figure 16: Temperature and equivalent particle absorption coefficient for SPOC stage 1 from FLUENT.

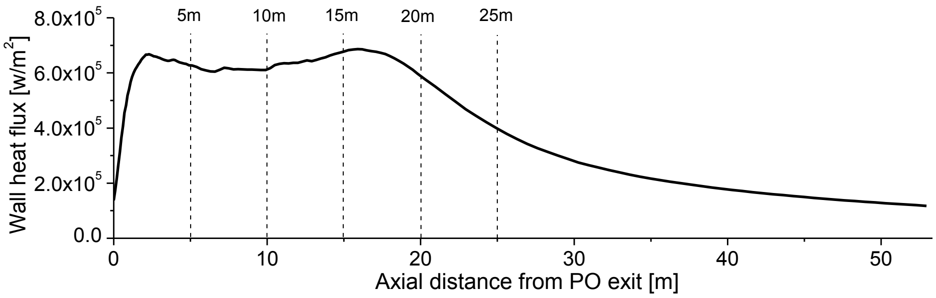

Figure 17: Wall heat flux for SPOC Stage 1 from FLUENT

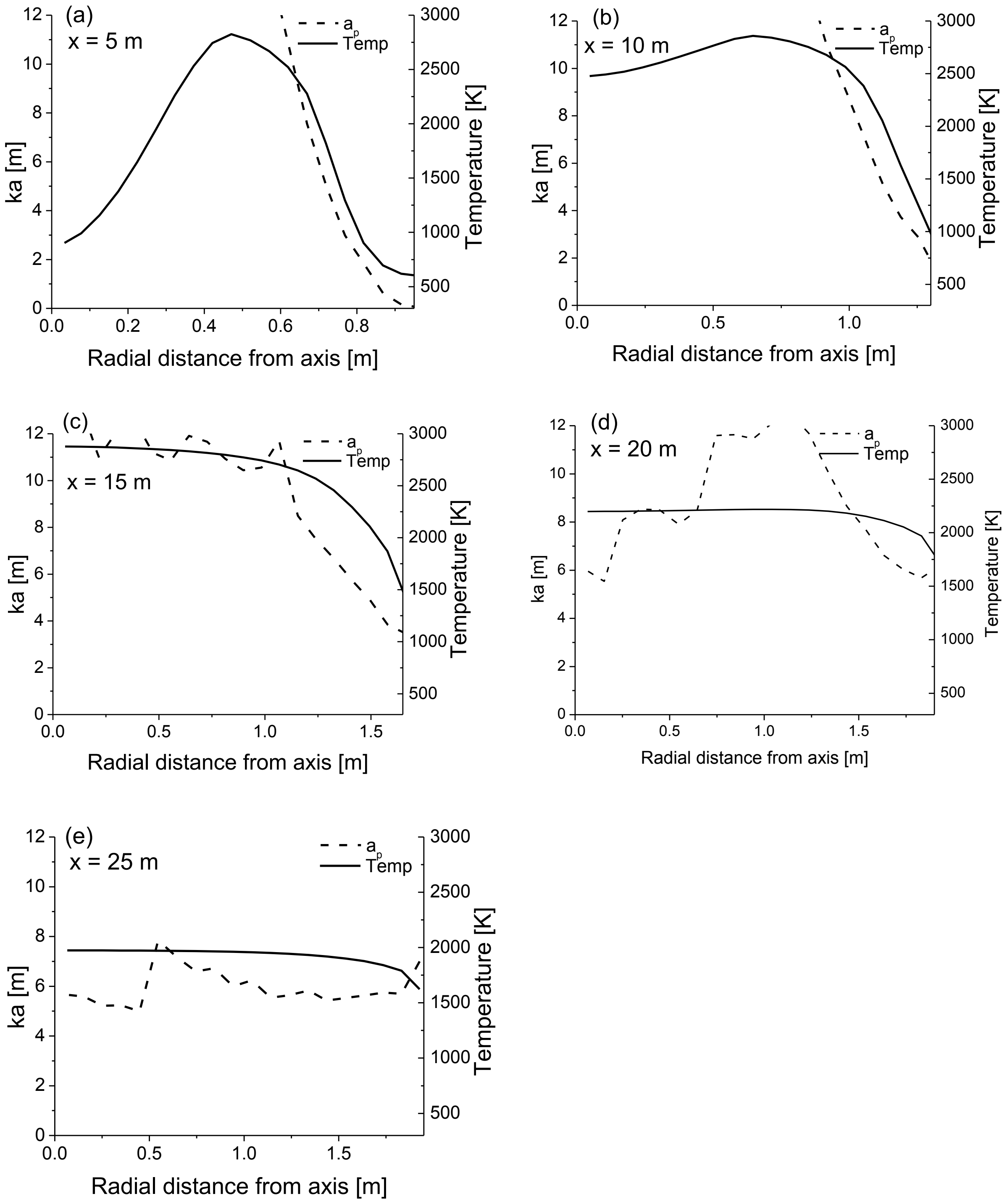

Figure 18: Temperature and equivalent particle absorption coefficient profiles in the radial direction for axial locations of a) x = 5, b) x = 10, c) x = 15, d) x = 20, and e) x = 25 m.

From the profiles of the temperature and the equivalent particle absorption, the boundaries and average temperature can be found and used to calculate the wall heat flux by applying the average temperature approximation (ATA) method. Figure 19 shows good agreement between the results obtained by the CFD simulation and ATA method, except for the axial location of 5 m. The reason is that the location (x=5) is so close to the burner that the inner boundary of ATA method locates in the positive-slope side of the flame, which makes ATA method at this location not as applicable as other locations.

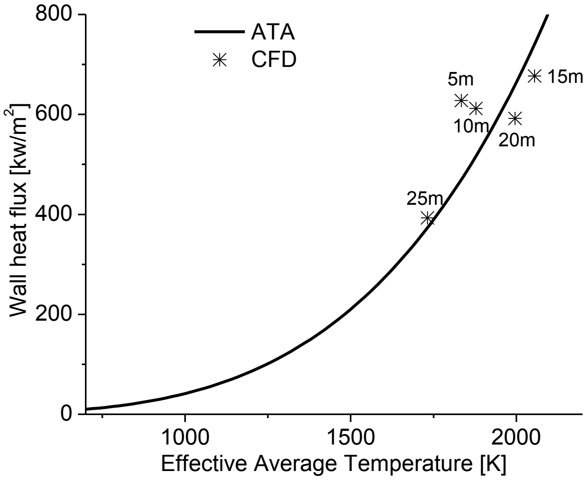

Figure 19: Wall heat flux values for the CFD simulation and ATA method.

CONCLUSION

Analysis of the Staged, Pressurized Oxy-Combustion (SPOC) process using ASPEN Plus has revealed the following:

- A combustion pressure of 15 bar is sufficient to recover nearly all of the latent heat from condensation of flue gas moisture, while enabling the integrated SOx and NOx removal chemistry.
- Further increase in pressure, up to 36 bar, is found to result in only a minor improvement in plant efficiency (approx. 0.14 percentage points) and the improvement with pressure is of diminishing returns.
- Dry nitrogen from the ASU and waste low-grade heat sources from the ASU and CPU compressors were identified, which may be utilized to dry coal to levels required for dense-phase pneumatic feeding. However, coal drying beyond what is necessary for feeding is of marginal benefit, since much of the latent heat from fuel moisture can be recovered in the direct contact cooler.
- The plant efficiency is reduced only slightly with increasing fuel moisture, until a saturation point is reached. For PRB coal, this point corresponds to approx. 29% moisture. For higher moisture contents, considering coal water slurries, the plant efficiency drops drastically above 29% since the amount of latent heat exceeds what can be incorporated into the steam cycle by feedwater heating.

A fundamental study of radiation in high-temperature, high-pressure, particle-laden flows was conducted to provide a more complete understanding of heat transfer in these unusual conditions and to allow for optimization. The important findings from this study are:

- At pressures relevant to SPOC, the combustion flue gas becomes very optically thick, due to the increase in char and ash particle volume fraction. Under these unique conditions, absorption and emission due to particles is a dominant factor for determining the wall heat flux.
- A mechanism is found to exist for “trapping” radiant energy within the high-temperature flame region, and controlling the transfer of this heat to the wall. This control arises, by design, from the highly non-uniform (non-premixed) combustion characteristics within the boiler, and the resulting gradients in temperature and particle concentration.
- A simple method for estimating the radiant heat flux to boiler surfaces is presented that may be widely applied in the design of pressurized coal combustion systems.

GRAPHICAL MATERIALS LIST

Tables

LIST OF ACRONYMS AND ABBREVIATIONS

EOR	Enhanced Oil Recovery
SPOC	Staged Pressurized Oxy-Combustion
NETL	National Energy Technology Laboratory
R&D	Research & Development
CFD	Computational Fluid Dynamics
DCC-HX	Direct Contact Column-Heat Exchanger
MACIC	Main Air Compressor Intercooler
BACIC	Booster Air Compressor Intercooler
OXYIC	Oxygen Compressor Intercooler
ASU	Air Separation Unit
RANS	Reynolds Averaged Navier-Stokes
SIMPLE	Semi-Implicit Method for Pressure Linked Equations
EDM	Eddy Dissipation Model
CPD	Chemical Percolation Devolatilization
RTE	Radiative Transfer Equation
DPM	Discrete Phase Model
DO	Discrete Ordinate
DRW	Discrete Random Walk
SO_x	Sulphur oxides
NOx	Nitrogen Oxides
CPU	Compressor Unit
BFW	Boiler Feed Water
LP	Low Pressure
k_a	Absorption coefficient
σ	Stefan-Boltzmann constant
T	Temperature
ζ	Optical thickness
whf	Wall Heat Flux
PRB	Powder River Basin

REFERENCES

1. *Quality Guidelines for Energy System Studies: Specifications for Selected Feedstocks; Report DOE/NETL - 341/081911.*, 2012, U.S. Department of Energy National Energy Technology Laboratory.
2. *Quality Guidelines for Energy System Studies: CO_2 Impurity Design Parameters; Report DOE/NETL - 341/081911.*, 2012, U.S. Department of Energy National Energy Technology Laboratory.
3. *Quality Guidelines for Energy System Studies: Process Modeling Design Parameters; Report DOE/NETL - 341/042613.*, 2013, U.S. Department of Energy National Energy Technology Laboratory.
4. *Quality Guidelines for Energy System Studies: Process Modeling Design Parameters, rev. 2; Report DOE/NETL - 341/081911.*, 2012, U.S. Department of Energy National Energy Technology Lab.
5. Gopan, A., et al., *Process design and performance analysis of a Staged, Pressurized Oxy-Combustion (SPOC) power plant for carbon capture.* Applied Energy, 2014. **125**(0): p. 179-188.
6. Edge, P., et al., *Combustion modelling opportunities and challenges for oxy-coal carbon capture technology.* Chemical Engineering Research and Design, 2011. **89**(9): p. 1470-1493.
7. Douglas Smoot, L., *Modeling of coal-combustion processes.* Progress in energy and combustion science, 1984. **10**(2): p. 229-267.
8. Yin, C., et al., *Use of numerical modeling in design for co-firing biomass in wall-fired burners.* Chemical engineering science, 2004. **59**(16): p. 3281-3292.
9. Eastwick, C., S. Pickering, and A. Aroussi, *Comparisons of two commercial computational fluid dynamics codes in modelling pulverised coal combustion for a 2.5 MW burner.* Applied Mathematical Modelling, 1999. **23**(6): p. 437-446.
10. Vuthaluru, R. and H. Vuthaluru, *Modelling of a wall fired furnace for different operating conditions using FLUENT.* Fuel processing technology, 2006. **87**(7): p. 633-639.
11. Ghenai, C. and I. Janajreh, *CFD analysis of the effects of co-firing biomass with coal.* Energy Conversion and Management, 2010. **51**(8): p. 1694-1701.
12. Backreedy, R., et al., *Co-firing pulverised coal and biomass: a modeling approach.* Proceedings of the Combustion Institute, 2005. **30**(2): p. 2955-2964.
13. Tian, Z.F., et al., *Comparison of two-equation turbulence models in simulation of a non-swirl coal flame in a pilot-scale furnace.* Combustion Science and Technology, 2009. **181**(7): p. 954-983.
14. Tian, Z.F., et al., *Modeling issues in CFD simulation of brown coal combustion in a utility furnace.* The Journal of Computational Multiphase Flows, 2010. **2**(2): p. 73-88.
15. Chen, L., S.Z. Yong, and A.F. Ghoniem, *Oxy-fuel combustion of pulverized coal: Characterization, fundamentals, stabilization and CFD modeling.* Progress in Energy and Combustion Science, 2012. **38**(2): p. 156-214.
16. Wolfgang Vieser, T.E., Florian Menter, *Heat transfer predictions using advanced two-equation turbulence models*, 2002.
17. Menter, F.R., *Influence of freestream values on k-omega turbulence model predictions.* AIAA Journal, 1992. **30**(6): p. 1657-1659.
18. Menter, F.R., *Two-equation eddy-viscosity turbulence models for engineering applications.* AIAA journal, 1994. **32**(8): p. 1598-1605.
19. Magnussen, B.F. and B.H. Hjertager, *On mathematical modeling of turbulent combustion with special emphasis on soot formation and combustion.* Symposium (International) on Combustion, 1977. **16**(1): p. 719-729.
20. Spalding, D. *Mixing and chemical reaction in steady confined turbulent flames*. in

Symposium (International) on Combustion. 1971. Elsevier.

21. Chen, L. and A.F. Ghoniem, *Simulation of Oxy-Coal Combustion in a 100 kWth Test Facility Using RANS and LES: A Validation Study.* Energy & Fuels, 2012. **26**(8): p. 4783-4798.
22. Fletcher, T.H., et al., *Chemical percolation model for devolatilization. 2. Temperature and heating rate effects on product yields.* Energy & Fuels, 1990. **4**(1): p. 54-60.
23. Genetti, D., T.H. Fletcher, and R.J. Pugmire, *Development and Application of a Correlation of 13C NMR Chemical Structural Analyses of Coal Based on Elemental Composition and Volatile Matter Content.* Energy & Fuels, 1998. **13**(1): p. 60-68.
24. *ANSYS Fluent 13.0 User's Guide*, 2010, ANSYS, Inc.
25. Baum, M. and P. Street, *Predicting the combustion behaviour of coal particles.* Combustion science and technology, 1971. **3**(5): p. 231-243.
26. Field, M.A., *Rate of combustion of size-graded fractions of char from a low-rank coal between 1 200 K and 2 000 K.* Combustion and Flame, 1969. **13**(3): p. 237-252.
27. Fluent, A., *ANSYS FLUENT Theory Guide: Version 13.0.* Ansys Inc., Canonsburg, 2010.
28. Chui, E.H. and G.D. Raithby, *COMPUTATION OF RADIANT HEAT TRANSFER ON A NONORTHOGONAL MESH USING THE FINITE-VOLUME METHOD.* Numerical Heat Transfer, Part B: Fundamentals, 1993. **23**(3): p. 269-288.
29. Raithby, G.D. and E.H. Chui, *A Finite-Volume Method for Predicting a Radiant Heat Transfer in Enclosures With Participating Media.* Journal of Heat Transfer, 1990. **112**(2): p. 415-423.
30. Friedlander, S.K., *Smoke, dust, and haze*. Vol. 198. 2000: Oxford University Press New York.
31. White, V., et al., *The Air Products Vattenfall Oxyfuel CO2 Compression and Purification Pilot Plant at Schwarze Pumpe.* Energy Procedia, 2013. **37**: p. 1490-1499.
32. Gopan, A., et al., *Process design and performance analysis of a Staged, Pressurized Oxy-Combustion (SPOC) power plant for carbon capture.* Applied Energy, 2014. **125**: p. 179-188.
33. Howell, J.R., R. Siegel, and M.P. Mengüç, *Thermal radiation heat transfer*. Fifth ed. 2010: CRC press.
34. Modest, M.F., *Radiative heat transfer*. 2013: Academic Press.

APPENDIX

Table A1. Properties of Wyodak/Anderson PRB sub-bituminous coal on an as-received basis[1]

Proximate Analysis	**PRB**
Moisture	27.42%
Volatile Matter	31.65%
Ash	4.50%
Fixed Carbon	36.43%
Total	100.00%
Ultimate Analysis	
Carbon	50.23%
Hydrogen	3.41%
Nitrogen	0.65%
Sulfur	0.22%
Chlorine	0.02%
Ash	4.50%
Moisture	27.42%
Oxygen	13.55%
Total	100.00%
Heating Value	**As-Received (Reported)**
HHV (kJ/kg)	20,469

Table A2. Site Conditions

Site Conditions	**Midwest ISO**
Elevation, m (ft)	0 (0)
Barometric Pressure, MPa (psia)	0.101 (14.7)
Design Ambient Dry Bulb Temperature, °C (°F)	15 (59)
Design Ambient Wet Bulb Temperature, °C (°F)	10.8 (51.5)
Design Ambient Relative Humidity, %	60
Cooling Water Temperature, °C (°F)	15.6 (60)
Air Composition, mass%	
H_2O	0.616
AR	1.280
CO_2	0.050
O_2	22.999
N_2	75.055
Total	100.00

Table A3. The CO_2 purity requirement for Enhanced Oil Recovery, and CO_2 purity achieved with the SPOC process

Component	**Enhanced Oil Recovery Target (Max. unless specified) [2]**	**SPOC Case**
CO_2	95% (min)	>99.9%
H_2O	300ppmwt	trace
N_2	1%	11ppb
O_2	100ppm	10ppm
Ar	1%	13ppm
H_2	1%	trace
CO	35ppm	trace
SO_2	100ppm	trace
NOx	100ppm	trace

Table A4 Summary of operating conditions

		Mass flow rate (kg/s)	O_2 content (vol.%)	CO_2 content (vol.%)	H_2O content (vol.%)	Temperature (K)
Stage 1	Coal	18.5				
	Primary stream	4.2	25	75	0	573
	Secondary stream	120	100	0	0	573
Stage 2	Coal	18.5				
	Primary stream	4.2	25	75	0	573
	Secondary stream	143	63.9	21.1	14.9	873
Stage 3	Coal	18.5				
	Primary stream	4.2	25	75	0	573
	Secondary stream	167.7	37.2	36.7	25.9	873
Stage 4	Coal	18.5				
	Primary stream	4.2	25	75	0	573
	Secondary stream	192.4	16.5	48.8	34.4	873